Differential algebra based magnetic field computations and accurate fringe field maps

Béla Erdélyi, Martin Berz and Michael Lindemann
Department of Physics and Astronomy and National Superconducting Cyclotron Laboratory, Michigan State University, East Lansing, MI 48824
(July 31, 2001)

41.85L, 85.25.L, 05.45.

Motivated by the dynamical studies of particle motion in magnetic fields, we develop the method of Differential Algebra (DA) based $3D$ magnetic field computation. It can be applied whenever an analytical model of a magnet is given, which usually consist of line wire currents. Such a model exists for most of the modern superconducting magnets. It is stressed that it is the only practically possible way to extract the multipoles and its derivatives, and hence the map, analytically to high order. We also elaborate on related topics like complexity of the problem, Maxwellification of fields, importance of vanishing curl, etc., and its applications to very accurate fringe field map computations.

I. INTRODUCTION

The performance of the modern high energy accelerators, such as the Large Hadron Collider to be built at CERN, depends critically on the field quality of the superconducting magnets employed to guide and focus the circulating beam [1]. The nonlinearities of these magnets drive resonances, rendering the motion of particles at large amplitudes unstable [2]. The shrinkage of the useful region in space, called the dynamic aperture, due to magnet nonlinearities is very detrimental to the stringent high luminosity requirements, so a careful design of these magnets is in order. The design is performed by sophisticated codes like ROXIE [3]. The accurate placement of the superconducting wires, followed by extensive optimization produces an analytical model of the magnet. Using the Biot-Savart law, the resulting magnetic field is computed on the surface of a coaxial cylinder with the optical axis, and subsequently Fourier analyzed numerically to reveal its multipole content. Several iterations are necessary to obtain a magnet model that satisfies the design specifications. However, once the magnet model is ready, the dynamical studies can use only the multipole data output of the magnet design codes, usually organized in tables. These contain the integrated values of the multipoles [4]. This is satisfactory for the dynamical studies of the so-called straight sections, where the fields are independent of the arclength s, which is used as the independent variable. However, it is not necessarily accurate enough for the end regions, the fringe fields, where the s dependence of the fields could result in unusual local dynamics not revealed by the integrated values. In the present paper we develop the theory that solves this problem by computing the magnetic fields based on Differential Algebraic methods. This method allows not just the extraction of the multipole strengths, but also their full s-dependence, allowing analytical computation of s-derivatives, which are necessary for "exact" fringe field map computations. The first steps in this direction have been done by Caspi [5]. Here we present the theory in its full generality. In section II we derive an improved, numerically stable version of the Biot-Savart law for straight line current wires in $3D$ and explain the principle of DA based field computation. Section III develops two methods for multipole extraction. The importance of enforcing Maxwell's equations is presented in Section IV. In fact, there are two methods to enforce Maxwell's equations: a local (IV A) and a global (IV B) approach. Finally, Section V contains examples of multipoles and applications to map computation.

II. BIOT-SAVART LAW AND FIELD COMPUTATION

The magnetic field computation is based on the Biot-Savart law. As will be shown in section III, to solve the equations of the motion, and hence to get the map of a magnetic element it is necessary to compute not just the value of the field at a certain point in space, but also its derivatives, that is its Taylor expansion. So, why do we want to use Differential Algebraic methods [6,7] to achieve this? In principle, it is possible to get the derivatives analytically and implement it in some code to evaluate them. We did it using Mathematica. The results are presented in Table I. We mention that the calculations have been done in only one variable (x), for one field component (B_y), and one single line current. On every computer we tried, Mathematica ran out of memory at the computation of the order 10 derivative. Therefore, it is clear that for realistic magnet models, consisting of several 10^5 line currents, in at least 2 variables up to high orders this way is practically intractable. As a comparison, Table II shows how fast is the DA method, and at the same time preserves the accuracy of the computed derivatives. Technically, all we need to get the

Taylor expansion of the field components around a specified point in space is the evaluation in DA of the Biot-Savart law.

While the exact form of the formula is not critical for the evaluation of the magnetic field value at a certain point in the space, as long it is mathematically accurate, it does have a significant influence when it is used to compute also the Taylor expansion of the field around a point. This is exactly what we attempt by evaluating it in DA. Some of the shortcomings of a naive implementation have been pointed out by Caspi [5]. Another numerical instability has been noticed by us when we utilized it at a point where some of the wire currents were exactly or almost colinear with the point of expansion. Therefore, we made several modifications to the standard form of the Biot-Savart law, and found a numerically stable version which has a good behavior in any situation.

As a consequence of Ampère's law, the elementary magnetic flux density at a point $\vec{r}$ generated by a filamentary current wire $d\vec{l}$ situated at $\vec{r}'$ is given by the Biot-Savart formula

$$d\vec{B} = \frac{\mu_0 I}{4\pi} \frac{d\vec{l} \times (\vec{r} - \vec{r}')}{|\vec{r} - \vec{r}'|^3} \tag{1}$$

To compute the magnetic field generated by an extended straight line current we parametrize the line by $\lambda \in [0,1]$ and define $\vec{r}'(\lambda) = \vec{r}_s + \lambda\vec{l}$ and $\vec{r}_e = \vec{r}_s + \vec{l}$, where $\vec{r}_s$, $\vec{r}_e$ represent the starting and endpoint respectively of the line current to the point $\vec{r}$.

Integrating over the line

$$\vec{B} = kI \int \frac{d\vec{l} \times \vec{r}'}{|\vec{r}'|^3} = kI \int_0^1 \frac{\vec{l} \times \left(\vec{r}_s + \lambda\vec{l}\right)}{\left|\vec{r}_s + \lambda\vec{l}\right|^3} d\lambda = kI \left(\vec{l} \times \vec{r}_s\right) \int_0^1 \frac{d\lambda}{\left|\vec{r}_s + \lambda\vec{l}\right|^3} \tag{2}$$

with $k = -\mu_0/(4\pi)$. Introducing the shorthand notations $a = |\vec{r}_s|^2$, $b = 2\vec{r}_s \cdot \vec{l}$, $c = \left|\vec{l}\right|^2$, the integral gives the result

$$\int_0^1 \frac{d\lambda}{(a + b\lambda + c\lambda^2)^{3/2}} = \frac{1}{b^2 - 4ac} \left(\frac{2b}{\sqrt{a}} - \frac{2b}{\sqrt{a+b+c}} - \frac{4c}{\sqrt{a+b+c}} \right) \tag{3}$$

While mathematically accurate, this formula exhibits several severe numerical pitfalls that restrict its direct practical use, in particular when high-order derivatives are to be computed. Indeed, first the formula apparently exhibits a problem of cancellation of closeby numbers if $b + c \ll a$. Introduction of the quantity $\varepsilon = (b + c)/a$ yields

$$\vec{B} = \frac{kI \left(\vec{l} \times \vec{r}_s\right)}{\sqrt{a}\,(b^2 - 4ac)} \left[2b \left(1 - \frac{1}{\sqrt{1+\varepsilon}} \right) - \frac{4c}{\sqrt{1+\varepsilon}} \right] \tag{4}$$

The first problem can be substantially alleviated now by observing that

$$1 - \frac{1}{\sqrt{1+\varepsilon}} = \frac{\varepsilon}{1 + \varepsilon + \sqrt{1+\varepsilon}} \tag{5}$$

which yields the formula

$$\vec{B} = \frac{kI \left(\vec{l} \times \vec{r}_s\right)}{\sqrt{a}\,(b^2 - 4ac)} \left[\frac{2b\varepsilon}{1 + \varepsilon + \sqrt{1+\varepsilon}} - \frac{4c}{\sqrt{1+\varepsilon}} \right] \tag{6}$$

However, there is a second numerical difficulty if the line current and the observation point are lying exactly or almost on the same line, because in this case b^2 and $4ac$ assume similar values, which makes the evaluation of $b^2 - 4ac$ prone to numerical inaccuracy. To avoid this effect we rewrite the formula in terms of the angle θ between $\vec{l}$ and $\vec{r}_s$. The relations among the angle and the products of vectors are

$$|\sin\theta| = \frac{\left|\vec{l} \times \vec{r}_s\right|}{\left|\vec{l}\right| \cdot |\vec{r}_s|} \qquad \text{and} \qquad \cos\theta = \frac{\vec{l} \cdot \vec{r}_s}{\left|\vec{l}\right| \cdot |\vec{r}_s|} \tag{7}$$

This implies the relationships

$$b^2 - 4ac = -4\left|\vec{r}_s\right|^2 \left|\vec{l}\right|^2 \sin^2\theta \tag{8}$$

$$\frac{2b\varepsilon}{1+\varepsilon+\sqrt{1+\varepsilon}} - \frac{4c}{\sqrt{1+\varepsilon}} = \frac{4\left|\vec{r}_s\right|\left|\vec{l}\right|\cos\theta\left(2\left|\vec{r}_s\right|\left|\vec{l}\right|\cos\theta+\left|\vec{l}\right|^2\right)}{\left|\vec{r}_e\right|\left(\left|\vec{r}_e\right|+\left|\vec{r}_s\right|\right)} - \frac{4\left|\vec{l}\right|^2\left|\vec{r}_s\right|}{\left|\vec{r}_e\right|}$$

Finally, we obtain the magnetic field expressed in terms of $\vec{r}_s$ and $\vec{l}$ as

$$\vec{B} = -\frac{kI\left(\vec{l}\times\vec{r}_s\right)}{\left|\vec{r}_s\right|^2\left|\vec{r}_s+\vec{l}\right|\left(\left|\vec{r}_s+\vec{l}\right|+\left|\vec{r}_s\right|\right)}\left[-\left|\vec{r}_s\right| + \frac{\left|\vec{r}_s\right|\cos^2\theta+\left|\vec{l}\right|\cos\theta-\left|\vec{r}_s+\vec{l}\right|}{\sin^2\theta}\right] \tag{9}$$

Denoting $\left|\vec{r}_s\right|\cos^2\theta + \left|\vec{l}\right|\cos\theta = \alpha$ and $\left|\vec{r}_s+\vec{l}\right| = \beta$, we manage to eliminate the $\sin^2\theta$ term in the denominator with the help of the identity $\alpha-\beta = \left(\alpha^2-\beta^2\right)/\left(\alpha+\beta\right)$. Direct calculation shows that $\alpha^2-\beta^2 = -\sin^2\theta\left(\left|\vec{r}_s\right|^2\cos^2\theta+\left|\vec{r}_s+\vec{l}\right|^2\right)$. Altogether we obtain the final result

$$\vec{B} = \frac{kI\left(\vec{l}\times\vec{r}_s\right)}{\left|\vec{r}_s\right|^2\left|\vec{r}_s+\vec{l}\right|\left(\left|\vec{r}_s+\vec{l}\right|+\left|\vec{r}_s\right|\right)}\left[\left|\vec{r}_s\right| + \frac{\left|\vec{r}_s\right|^2\cos^2\theta+\left|\vec{r}_s+\vec{l}\right|^2}{\left|\vec{r}_s\right|\cos^2\theta+\left|\vec{l}\right|\cos\theta+\left|\vec{r}_s+\vec{l}\right|}\right] \tag{10}$$

The only case where this is numerically unstable is when $\left|\vec{r}_s\right|\cos^2\theta+\left|\vec{l}\right|\cos\theta+\left|\vec{r}_s+\vec{l}\right|$ approaches zero, that is $\theta\to\pi$ and $\left|\vec{r}_s\right| \le \left|\vec{l}\right|$; but this corresponds to a point in the close proximity of the wire.

The necessary ingredients for the DA field calculation are the above formula and the analytic model of the magnet, consisting of line wire currents. To this end, the entire field in space is calculated by summing up the fields created by wire currents. At each step, the evaluation of (10) in DA yields not only the value of the magnetic field at the respective point, but also its derivatives, that is the Taylor expansion with respect to coordinates. The result for the return end of the Large Hadron Collider's High Gradient Quadrupole, up to order 3, is presented in Table III. The correctness of our results have been checked against data obtained from Fermilab. The Fermilab data contains the values of the components of the field on the surface of a coaxial cylinder with the optical axis, and have been supplied by G. Sabbi.

To show that the Biot-Savart law implementation based on eq. (10) is much more stable then, for example, based on eq. (6), we use as an indicator the s component of the curl of the field. From Table IV it is clear that the naive implementation goes wrong as low as second order in the curl. Due to lack of space, we presented the result only up to order 3, but our results show that the behavior of eq. (10) is good up to very high orders. Also, we mention that probably this is the most straightforward and accurate way to compute the curl and hence verify whether Maxwell's equations are satisfied.

III. MULTIPOLE EXTRACTION ALGORITHMS

A. The direct method

Using the field computation of the preceding section, it is possible to extract the multipole content of magnetic fields directly, in a very elegant way that is arbitrary in order. In the following we assume straight optical axis. In the divergence-free, curl-free region of the magnets it is possible to derive the magnetic field components from a magnetic scalar potential that satisfies the Laplace equation. The general solution expanded in normal and skew components has the form

$$V_B = \sum_{k,l=0}^{\infty}\left(b_{k,l}(s)\sin l\phi + a_{k,l}(s)\cos l\phi\right)r^k \tag{11}$$

Defining $\theta_{k,l}(s)$ and $M_{k,l}(s)$ by

$$\tan\theta_{k,l}(s) = -\frac{b_{k,l}(s)}{a_{k,l}(s)} \qquad M_{k,l}(s) = \sqrt{b_{k,l}^2(s)+a_{k,l}^2(s)} \tag{12}$$

we have an equivalent form

$$V_B = \sum_{k,l=0}^{\infty} M_{k,l}(s) \cos\left(l\phi + \theta_{k,l}(s)\right) r^k \tag{13}$$

which shows that any normal (skew) component can be obtained from the corresponding skew (normal) component by an s-dependent rotation around the s axis. The link between the two forms in the other direction is

$$\begin{aligned} b_{k,l}(s) &= -M_{k,l}(s) \sin\theta_{k,l}(s) \\ a_{k,l}(s) &= M_{k,l}(s) \cos\theta_{k,l}(s) \end{aligned} \tag{14}$$

Inserting (11) in the Laplace equation in cylindrical coordinates

$$\Delta V_B = \frac{1}{r}\frac{\partial}{\partial r}\left(\frac{r\partial V_B}{\partial r}\right) + \frac{1}{r^2}\frac{\partial^2 V_B}{\partial \phi^2} + \frac{\partial^2 V_B}{\partial s^2} = 0 \tag{15}$$

we obtain

$$\sum_{k,l=0}^{\infty} \left[\left(b_{k,l}(s)(k^2-l^2) + b''_{k-2,l}(s)\right)\sin l\phi + \left(a_{k,l}(s)(k^2-l^2) + a''_{k-2,l}(s)\right)\cos l\phi\right] r^{k-2} = 0 \tag{16}$$

using the convention that the coefficients vanish for negative indices. Due to the fact that the above equation must hold for every r and ϕ, and the sin and cos are linearly independent

$$\begin{aligned} b_{k,l}(s)(k^2-l^2) + b''_{k-2,l}(s) &= 0 \\ a_{k,l}(s)(k^2-l^2) + a''_{k-2,l}(s) &= 0 \end{aligned} \tag{17}$$

Furthermore, it can be shown that the following recurrence relations hold

$$b_{l+2n,l}(s) = \frac{b^{(2n)}_{l,l}(s)}{\Pi_{\nu=1}^{n}\left(l^2-(l+2\nu)^2\right)} \qquad a_{l+2n,l}(s) = \frac{a^{(2n)}_{l,l}(s)}{\Pi_{\nu=1}^{n}\left(l^2-(l+2\nu)^2\right)} \tag{18}$$

and the coefficients that cannot be obtained by these relations are zero. The $b_{l,l}(s)$, $a_{l,l}(s)$ are called normal and skew (true) multipoles respectively, while the terms that contain s-derivatives are called pseudo-multipoles. It is worth mentioning that, as one can see from eq. (12), the recurrence relations (18) do not hold in general for $M_{k,l}(s)$. However, when the $\theta_{k,l}$'s are s-independent, eq. (18) holds for $M_{k,l}(s)$. Inserting relations (18) in (11), we get for the potential

$$V_B = \sum_{l=0}^{\infty} \left(f_l(r,s)\sin l\phi + g_l(r,s)\cos l\phi\right) r^l \tag{19}$$

where

$$\begin{aligned} f_l(r,s) &= \sum_{n=0}^{\infty} b_{l+2n,l}(s) r^{2n} = \sum_{n=0}^{\infty} \frac{b^{(2n)}_{l,l}(s)}{\Pi_{\nu=1}^{n}\left(l^2-(l+2\nu)^2\right)} r^{2n} \\ &= b_{l,l}(s) - \frac{b^{(2)}_{l,l}(s)}{4(l+1)} r^2 + \frac{b^{(4)}_{l,l}(s)}{32(l+1)(l+2)} r^4 - \frac{b^{(6)}_{l,l}(s)}{384(l+1)(l+2)(l+3)} r^6 + \ldots \\ g_l(r,s) &= \sum_{n=0}^{\infty} a_{l+2n,l}(s) r^{2n} = \sum_{n=0}^{\infty} \frac{a^{(2n)}_{l,l}(s)}{\Pi_{\nu=1}^{n}\left(l^2-(l+2\nu)^2\right)} r^{2n} \\ &= a_{l,l}(s) - \frac{a^{(2)}_{l,l}(s)}{4(l+1)} r^2 + \frac{a^{(4)}_{l,l}(s)}{32(l+1)(l+2)} r^4 - \frac{a^{(6)}_{l,l}(s)}{384(l+1)(l+2)(l+3)} r^6 + \ldots \end{aligned} \tag{20}$$

The functions $f_l(r,s)$ and $g_l(r,s)$ represent the "out of axis" expansion of the multipoles. The magnetic field components in cylindrical coordinates can be calculated using the well known formulas

$$B_r = -\frac{\partial V_B}{\partial r} \tag{21}$$
$$B_\phi = -\frac{1}{r}\frac{\partial V_B}{\partial \phi}$$
$$B_s = -\frac{\partial V_B}{\partial s}$$

resulting the expressions

$$B_r(r,\phi,s) = \tilde{g}_0(r,s) + \sum_{l=1}^{\infty}\left[\tilde{f}_l(r,s)\sin l\phi + \tilde{g}_l(r,s)\cos l\phi\right] r^{l-1} \tag{22}$$
$$B_\phi(r,\phi,s) = \sum_{l=1}^{\infty}\left[l\left(f_l(r,s)\cos l\phi - g_l(r,s)\sin l\phi\right)\right] r^{l-1}$$
$$B_s(r,\phi,s) = \sum_{l=0}^{\infty}\left[f_l^{'}(r,s)\sin l\phi + g_l^{'}(r,s)\cos l\phi\right] r^{l}$$

where prime denotes derivative with respect to s and

$$\tilde{f}_l(r,s) = \sum_{n=0}^{\infty}(l+2n)b_{l+2n,l}(s)r^{2n} = \sum_{n=0}^{\infty}\frac{(l+2n)b_{l,l}^{(2n)}(s)}{\Pi_{\nu=1}^{n}\left(l^2-(l+2\nu)^2\right)}r^{2n} \tag{23}$$
$$= lb_{l,l}(s) - \frac{(l+2)b_{l,l}^{(2)}(s)}{4(l+1)}r^2 + \frac{(l+4)b_{l,l}^{(4)}(s)}{32(l+1)(l+2)}r^4 - \frac{(l+6)b_{l,l}^{(6)}(s)}{384(l+1)(l+2)(l+3)}r^6 + \ldots$$
$$\tilde{g}_l(r,s) = \sum_{n=0}^{\infty}(l+2n)a_{l+2n,l}(s)r^{2n} = \sum_{n=0}^{\infty}\frac{(l+2n)a_{l,l}^{(2n)}(s)}{\Pi_{\nu=1}^{n}\left(l^2-(l+2\nu)^2\right)}r^{2n}$$
$$= la_{l,l}(s) - \frac{(l+2)a_{l,l}^{(2)}(s)}{4(l+1)}r^2 + \frac{(l+4)a_{l,l}^{(4)}(s)}{32(l+1)(l+2)}r^4 - \frac{(l+6)a_{l,l}^{(6)}(s)}{384(l+1)(l+2)(l+3)}r^6 + \ldots$$

It can be seen that every multipole, except for $l=0$, is multiplied by r^{l-1}. For the special case $l=0$, we get

$$B_r(r,s) = \tilde{g}_0(r,s) = -\sum_{k=1}^{\infty}(-1)^{k+1}\frac{k}{2^{2k-1}k!k!}a_{0,0}^{(2k)}(s)r^{2k-1} \tag{24}$$
$$B_\phi(r,s) = 0$$
$$B_s(r,s) = -\sum_{k=0}^{\infty}(-1)^{k+1}\frac{1}{2^{2k}k!k!}a_{0,0}^{(2k+1)}(s)r^{2k}$$

In the DA picture, the field calculations are done locally, as a Taylor expansion of the field with respect to Cartesian coordinates x, y, s. Hence, we need the equations relating the cylindrical and Cartesian components of the magnetic field.

$$B_x(r,\phi,s) = B_r(r,\phi,s)\cos\phi - B_\phi(r,\phi,s)\sin\phi \tag{25}$$
$$B_y(r,\phi,s) = B_r(r,\phi,s)\sin\phi + B_\phi(r,\phi,s)\cos\phi$$

and $B_s(r,\phi,s)$ is unchanged. Obviously, if we evaluate the above equations in the midplane ($y=\phi=0$), then

$$B_r(r,\phi=0,s)\mid_{r\mapsto x} = B_x(x,y=0,s) \tag{26}$$
$$B_\phi(r,\phi=0,s)\mid_{r\mapsto x} = B_y(x,y=0,s)$$

So, all the information we need to extract the multipoles up to the order of calculation is in the Cartesian components of the fields in the midplane

$$B_x(x,y=0,s) = \tilde{g}_0(x,s) + \sum_{l=1}^{\infty}\tilde{g}_l(x,s)\cdot x^{l-1} \tag{27}$$
$$B_y(x,y=0,s) = \sum_{l=1}^{\infty} l f_l(x,s)\cdot x^{l-1}$$

This is possible due to the previously mentioned fact that any multipole strength of order l is multiplied by x^{l-1}. Starting at $l = 1$, $a_{1,1}(s)$ is extracted as the x-independent part of B_x, and analogously $b_{1,1}(s)$ from B_y. Evaluating $a_{1,1}(s)$ and $b_{1,1}(s)$ at $s = 0$ yields the skew and normal dipole component. From $a_{1,1}(s)$ and $b_{1,1}(s)$ the functions $f_1(x,s)$, $\tilde{g}_1(x,s)$ are generated up to the order of calculation and subtracted from $B_x(x, y = 0, s)$, and $B_y(x, y = 0, s)$ respectively. This cancels the pseudo-multipoles generated by the s-dependence of $a_{1,1}(s)$ and $b_{1,1}(s)$ (eq. (18)), which otherwise would make the distinction between sextupole terms and pseudo-dipole terms impossible. The procedure can be iterated for the higher order multipoles, up to the order of calculation. After the k-th step, the remainder of the field components should contain just $(k+1)$-th and higher order multipoles.

However, there is an additional problem in the case of solenoidal fields (case $l = 0$). In this case we have an $a_{0,0}(s)$ in the potential, but its contribution vanishes from the field components B_x and B_y, so the function $\tilde{g}_0(x,s)$ cannot be generated from the information available in B_x and B_y. Fortunately, it can be generated from the B_s component, which evaluated at $x = y = 0$ yields $a'_{0,0}(s)$. From this function we can calculate $a_{0,0}(s)$ up to a constant and generate the $l = 0$ contribution to B_x, $\tilde{g}_0(x,s)$. Once this is subtracted from B_x, the method works as previously described, starting with $l = 1$.

Finally, two notes: the method relies on the fact that the magnetic field can be generated by a magnetic scalar potential that satisfies the Laplace equation. Therefore, it is really important that the curl of the field vanishes. If the fields are calculated from line currents by the Biot-Savart law, that means that the model should consist only of closed circuits to ensure vanishing curl. Maxwellification of the field ensures a better numerical stability of the algorithm. Secondly, only in the regions where the magnetic field is not s-dependent the functions f_l and g_l are equal to the true multipoles, and $lf_l = \tilde{f}_l$, $lg_l = \tilde{g}_l$, an assumption that is sometimes made even for the s-dependent region too.

B. Multipole extraction by analytical Fourier transform

There is an alternate way to extract the multipoles. The field computation being performed in COSY in Cartesian coordinates (x, y, s), it is possible to perform an analytical pseudo-Fourier transform, meaning a series of coordinate transformation in DA, keeping the r and s dependence. This is solved by our S-Dependent Differential Algebraic Analytical Fourier Transform presented below.

Initially, the field components are in the form of eq. (A1). The first transformation is $(x, y, s) \mapsto (r, \cos\phi, \sin\phi, s)$ by $x = r\cos\phi$ and $y = r\sin\phi$. At the same time, using eq. (A2) we switch to cylindrical coordinates, obtaining the field components in the form of eq. (A3). Note that we are going from a 3 variable representation to a 4 variable one, therefore some of the information in the new representation will turn out to be redundant for our purpose. The next transformation is $(r, \cos\phi, \sin\phi, s) \mapsto (r, e^{i\phi}, e^{-i\phi}, s)$, that is the exponential, and obviously a complex representation, using $\cos\phi = \left(e^{i\phi} + e^{-i\phi}\right)/2$ and $\sin\phi = \left(e^{i\phi} - e^{-i\phi}\right)/(2i)$.

We proved previously that it does not matter which field component is used for Fourier transformation, so assume that we are working with B_r. Then, we have it at this stage in the form $B_r(r, e^{i\phi}, e^{-i\phi}, s)$.

Now, in principle, it is possible to recombine various products of powers of $e^{i\phi}$ and $e^{-i\phi}$ to trigonometric functions involving multiple angles. However, the key point is to notice that we can obtain the true multipoles by setting $e^{i\phi} = 0$. This is true due to the fact that all the terms of the form $e^{iq\phi}e^{-ip\phi}$, with $q, p \neq 0$, are responsible for the pseudo-multipoles. This becomes clear if one takes a closer look at eq. (A5). By setting $e^{i\phi}$ to zero we get rid of all the pseudo-multipole terms and we are going back to a 3 variable representation

$$B_r(r, e^{-i\phi}, s) = \sum_{l=1}^{n+1} z_l(s) e^{-il\phi} r^{l-1} \tag{28}$$

where $z_l(s)$ are complex functions of s. By comparison with eq. (A12) it is obvious that one term of eq. (28) can come only from $[A_l(s)\cos l\phi + B_l(s)\sin l\phi]\, r^{l-1}$, which also can be expressed as

$$\left[e^{-il\phi}\left(\frac{B_l(s)}{2} + i\frac{A_l(s)}{2}\right) + e^{il\phi}\left(\frac{B_l(s)}{2} - i\frac{A_l(s)}{2}\right)\right] r^{l-1} \tag{29}$$

After setting $e^{il\phi}$ to zero and comparison with eq. (28) we obtain the result $B_l(s) = 2\,\mathrm{Re}\,(z_l(s))$ and $A_l(s) = 2\,\mathrm{Im}\,(z_l(s))$. As a final step, we take the true multipoles as given by

$$\begin{aligned} b_{l,l}(s) &= \frac{2}{l}\,\mathrm{Re}\,(z_l(s)) \\ a_{l,l}(s) &= \frac{2}{l}\,\mathrm{Im}\,(z_l(s)) \end{aligned} \tag{30}$$

IV. ENFORCING MAXWELL'S EQUATIONS

A. Local Maxwellification

Given a magnet model consisting of line currents, it is possible to compute the magnetic field generated by the Biot-Savart law in the DA framework as a local Taylor expansion with respect to the Cartesian coordinates (x, y, s), as has been demonstrated in section II. The magnetic field should be divergence and curl-free in the regions of interest, as implied by the Maxwell equations in a source-free region: $\nabla \cdot \vec{B} = 0$ and $\nabla \times \vec{B} = 0$. This is the case only when the magnet model consist of closed loops of current. Realistic magnet models, as for example the LHC HGQ end regions as modeled by the code ROXIE and supplied by G. Sabbi of FNAL, are not closed due to presence of image currents, "leads" and separate treatment of the two end regions (lead end and return end). One way to fix this problem is to input as much physical intuition as possible to close the magnet model, compute the field generated by this model, which should differ as little as possible from the original model. This is the first step of Maxwellification. Obviously, the solution is not unique due to infinitely many ways of closing the model. The closing is important to guarantee vanishing curl, as it is required by the Maxwell equations, and in this case the field is derivable from a scalar potential. From the DA computational point of view it is also important, because it is enough to compute the field components only in the midplane (see section III). The computer time needed for computing a magnet model of several 10^5 line currents to high order in one end region of the LHC HGQ's scales much worse with the increase of the number of variables than with the increase of line currents, which should be linear. Besides computer time, the second step of the Maxwellification provides a way to correct for small computational errors or magnet model imperfections. One specific example is the method of the next section. Although the curl is already small, as shown in Table IV, the numerical stability of the multipole extraction algorithm is improved by local Maxwellification of the field, which is described below.

If we restrict ourselves to elements with straight optical axis for simplicity, the second step of Maxwellification proceeds as follows. Given $B_x(x, 0, s)$, $B_y(x, 0, s)$, $B_s(x, 0, s)$ ($y = 0$ representing the midplane) we can compute the field components in the whole space. From a scalar potential $V(x, y, s)$ that satisfies the Laplace equation

$$\frac{\partial^2 V(x,y,s)}{\partial x^2} + \frac{\partial^2 V(x,y,s)}{\partial y^2} + \frac{\partial^2 V(x,y,s)}{\partial s^2} = 0 \tag{31}$$

the field results from the well-known relation $\vec{B}(x, y, s) = \nabla V(x, y, s)$ (we neglect the sign which is irrelevant in our discussion). We transform the Laplace equation to a fixed point problem by isolating the y derivative term and integrating with respect to y

$$\frac{\partial^2 V(x,y,s)}{\partial y^2} = -\left(\frac{\partial^2 V(x,y,s)}{\partial x^2} + \frac{\partial^2 V(x,y,s)}{\partial s^2}\right) \tag{32}$$

$$\Rightarrow \qquad \int_0^{y'} \frac{\partial^2 V(x,y'',s)}{\partial y''^2} dy'' = -\int_0^{y'} \left(\frac{\partial^2 V(x,y'',s)}{\partial x^2} + \frac{\partial^2 V(x,y'',s)}{\partial s^2}\right) dy'' \tag{33}$$

$$\Rightarrow \qquad \frac{\partial V(x,y',s)}{\partial y'} = \left.\frac{\partial V(x,y'',s)}{\partial y''}\right|_{y''=0} - \int_0^{y'} \left(\frac{\partial^2 V(x,y'',s)}{\partial x^2} + \frac{\partial^2 V(x,y'',s)}{\partial s^2}\right) dy''$$

Integrating once more

$$\int_0^y \frac{\partial V(x,y',s)}{\partial y'} dy' = V(x,y,s) - V(x,0,s) \tag{34}$$

$$\Rightarrow V(x,y,s) = V(x,0,s) + \int_0^y \left.\frac{\partial V(x,y'',s)}{\partial y''}\right|_{y''=0} dy' - \int_0^y \int_0^{y'} \left(\frac{\partial^2 V(x,y,s)}{\partial x^2} + \frac{\partial^2 V(x,y,s)}{\partial s^2}\right) dy'' dy'$$

we obtain a fixed point problem for $V(x, y, s)$. In the DA picture it converges to the exact solution in $[n/2]$ steps, where n is the order of computation [8]. Since the Laplace equation is a second order PDE, we need two initial conditions. One is immediate from

$$\int_0^y \left.\frac{\partial V(x,y'',s)}{\partial y''}\right|_{y''=0} dy' = y B_y(x,0,s) \tag{35}$$

because by definition $\partial V/\partial y = B_y$. This is already known, and the other initial condition to be calculated is the potential in the midplane $V(x,0,s)$.

In the ideal case the potential in the midplane is computed by a path integral, along an arbitrary path. This is the case when the curl of the initial field is exactly vanishing. Due to various causes previously mentioned this is almost never true. Nevertheless, the curl it is usually small. Then, one should use a path along which the field is deemed more accurately computed, yielding a potential, and subsequently field components that are close to the original, and curl that is almost vanishing. Hence the name Maxwellification.

Most of the time it is not obvious where the fields are computed more accurately. Then one could try different paths and choose the one giving the smallest curl. Convenient choices of paths are along the sides or diagonal of a rectangle in the midplane with opposite corners at $(0,0)$ and (x,s). In the midplane we have $dV(\vec{r}) = \vec{B}(\vec{r}) \cdot d\vec{r}$, where $\vec{r} = (x,0,s)$. Integrating, we get

$$V(\vec{r}) = V(\vec{0}) + \int_0^{\vec{r}} \vec{B}\,(\vec{r}\,') \cdot d\vec{r}\,' \tag{36}$$

We can neglect the immaterial constant $V(\vec{0})$, and integration along the sides in one direction gives

$$V(x,0,s) = \int_0^x B_x(x',0,0)dx' + \int_0^s B_s(x,0,s')ds' \tag{37}$$

Integration along the sides in the other direction gives

$$V(x,0,s) = \int_0^s B_s(0,0,s')ds' + \int_0^x B_x(x',0,s)dx' \tag{38}$$

For integration along the diagonal we set $\vec{r}\,' = \lambda\vec{r}$ with $\lambda \in [0,1]$. Then, $d\vec{r}\,' = \vec{r}d\lambda$ and

$$V(x,0,s) = x\int_0^1 B_x(\lambda x,0,\lambda s)d\lambda + s\int_0^1 B_s(\lambda x,0,\lambda s)d\lambda \tag{39}$$

One can check by direct calculation that indeed $B_x(x,0,s) = \frac{\partial V(x,0,s)}{\partial x}$ and $B_s(x,0,s) = \frac{\partial V(x,0,s)}{\partial s}$. This completes the Maxwellification procedure. Once we have $V(x,y,s)$ we can compute the field components satisfying Maxwell's equations in the whole region of interest.

In DA the field components are computed as local Taylor expansions, so the method provides a local Maxwellification. That's why beside choosing the right path is might be useful to average over a certain region to decide which approach is the best. Finally, it should be obvious how to extend all the equations in the case of full $3D$ Maxwellification, if originally the field components are given in all 3 variables (x,y,s). For example, (37) is extended as

$$V(x,y,s) = \int_0^x B_x(x',0,0)dx' + \int_0^s B_s(x,0,s')ds' + \int_0^y B_y(x,y',s)dy' \tag{40}$$

and in the same way in other cases. In this situation, of course, there are many more path choices and no fixed point transformation of the Laplace equation is needed.

As an example, in Table V we present the s component of the curl of the Maxwellified field of Table III. We mention that the now we present the results up to order 12 in the curl and the first non-vanishing element occurs at order 6. Also, notice the improvement in comparison with the curl in Table IV.

B. Global Maxwellification

We saw that local Maxwellification is possible based on a closed magnet model consisting of line currents. One might imagine cases when the magnet model is not closed, and for some reason it is practically impossible to close it, or the actual closings change the original fields significantly. For such cases the S-Dependent Differential Algebraic Analytical Fourier Transform (SDDAAFT) provides a way for global Maxwellification and minimal modification of the original fields in a neighborhood of the optical axis. The only drawback compared to the previous method is that we need the field computation of the unclosed model in all 3 variables (x,y,s), which implies increased computer time.

We start with the magnetic field vector $\vec{B}(x,y,s)$ representing the field of an unclosed magnet model computed using Biot-Savart law. Therefore, $\nabla \cdot \vec{B} = 0$ and $\nabla \times \vec{B} \neq 0$. Then, exist another vector $\vec{R}(x,y,s)$, which stands for the field generated by fictitious line currents representing the closings of the model. Obviously, $\vec{R}$ is not unique, due to infinitely many possibilities of closing. It follows that $\nabla \cdot \vec{R} = 0$ and $\nabla \times \left(\vec{B} + \vec{R}\right) = 0$. Taking the cross product $\nabla \times \nabla \times \left(\vec{B} + \vec{R}\right) = \nabla \left(\nabla \cdot \left(\vec{B} + \vec{R}\right)\right) - \Delta \left(\vec{B} + \vec{R}\right) = 0$, we obtain $\Delta \left(B_i + R_i\right) = 0$, B_i and R_i being the components in cylindrical coordinates of $\vec{B}$ and $\vec{R}$. Now, we know from the direct method what is the structure of a function in cylindrical coordinates that satisfies the Laplace equation. Hence, we get

$$R_i(r,\phi,s) = \sum_{l=0}^{\infty} \left(f_{i,l}(r,s)\sin l\phi + g_{i,l}(r,s)\cos l\phi\right) r^l - B_i(r,\phi,s) \tag{41}$$

Apparently, we get the smallest R_i in the vicinity of the optical axis if we choose the free parameters in $f_{i,l}(r,s)$ and $g_{i,l}(r,s)$, the true multipoles, such that they cancel the corresponding terms in B_i. This way we fix uniquely the true multipoles, that are anyway the dominating part, and let R_i to contribute only for the pseudo-multipole parts. Here we define as being a true multipole of order l the s-dependent function that is the coefficient of $r^{l-1}\cos l\phi$ or $r^{l-1}\sin l\phi$ respectively in the expression of B_i. This definition makes sense, as this is the case in general when the fields are derivable from a magnetic scalar potential.

Once the principle is understood, in practice we do not need to calculate explicitly R_i. It is enough to have B_i and extract the relevant terms, the true multipoles, then the out of axis expansion is performed, the potential is built up and the new fields are computed. The new fields will satisfy Maxwell's equation, hence the name global Maxwellification.

Still, one thing remains to be proved. The solution is really unique if we prove that the true multipoles are invariant with respect to which component of the original field we choose, B_r or B_ϕ. This result is easily obtained in case we impose the vanishing curl and divergence conditions, as has been shown in the direct method. It can be shown that this is the case without imposing any constraints on the coefficients. This is the subject of Appendix A. Also, in the same Appendix we stress the importance of the constraints imposed by the vanishing curl.

All the methods described have been implemented in the DA based code COSY INFINITY [9–11].

V. EXAMPLES AND COMPUTATION OF MAPS

Using the methods developed in the present paper, we computed the multipole strengths as a function of s for the LHC interaction region's High Gradient Quadrupoles. These quadrupoles have two end regions, the lead end and the return end, where the fields are s-dependent. We computed the multipoles up to 28-poles for both ends. The field computation has been performed up to order 13, at 1 cm equally spaced points along the optical axis. In the following we restrict ourselves to present the results for the lead end only. Figure 1 shows the extracted normal and skew quadrupole, duodecapole, and 20-pole components.

As previously mentioned, the map computation needs also the s-derivatives of the multipoles. These are easily obtained as a by-product of the multipole extraction algorithms, because we always keep their s dependence. Derivative computation in DA in an elementary operation. It yields very accurate results without the need to resort to numerical differentiation. Some of the s derivatives of multipoles presented in Figure 1 are shown in Figure 2 and Figure 3. The multipoles and their derivatives have been interpolated for plotting by a derivative preserving interpolation scheme. Also, the two multipole extraction algorithms were checked against each other and found to be in complete agreement.

The importance of vanishing curl has been stressed at several points throughout the paper. To show the influence on the extracted quadrupole strength and its derivatives of the effect of non-vanishing curl, we compare two cases: multipole extracted from a magnet model that generates field with non-vanishing curl, and multipole extracted from the same magnet model after all the open ended wires have been closed at "infinity" (meaning far away from the observation points). The result is contained in Figure 4. It can be seen that although the agreement is still pretty good for the multipoles, the differences are amplified for the derivatives.

As an application we describe very accurate high-order map computations of s-dependent fields. There are two ways to calculate maps. In the first case the following three steps are needed: using the analytical magnet model, the field expansions at selected support points along the optical axis are computed. In case it is necessary, the Maxwellification is included in this step. Then follows the extraction of the multipoles. Finally, the multipoles are interpolated by Gaussian interpolation [12], and using the integration algorithm of COSY described in [11], the map is generated.

The alternate way's first step is the same. However, the scalar potential at support points is anyway computed in the process of Maxwellification. We use this potential to integrate the equations of the motion, with an interpolation scheme that preserves the derivatives at the support points, yielding the map.

Both methods have been implemented in COSY and they give essentially the same results. Especially at high orders the Gaussian method is faster, due to the smoothing properties of Gaussian interpolation [12]. Although to list the whole map it would be too long, to get a feeling of the resulting fringe field maps for the above mentioned end regions we list the opening aberrations in both ends up to order 8 in Table VI. Once we have the maps, they can be employed for dynamics studies, which is actually the final purpose of the whole theory and methods developed in the present paper. We applied the methods to study the fringe field effects in the LHC. Some of the results can be found in [13].

ACKNOWLEDGMENTS

We would like to thank G. Sabbi for many useful discussions and the considerable amount of data supplied for the Large Hadron Collider's interactions region High Gradient Quadrupoles.

---

[1] The LHC Study Group, The Large Hadron Collider, Conceptual Design, Technical Report No. AC/95-05, CERN (unpublished).
[2] F. Pilat et al., in *Proceedings EPAC* (IOP, Stockholm, Sweden, 1998).
[3] S. Russenschuck, Technical Report No. CERN AT/95-39, CERN (unpublished).
[4] G. Sabbi, Technical Report No. TD-97-040, Fermi National Accelerator Laboratory (unpublished).
[5] S. Caspi et al., Technical Report No. LBL-32624, L. Berkley Laboratory (unpublished).
[6] M. Berz, Nuclear Instruments and Methods **A298**, 426 (1990).
[7] M. Berz, Particle Accelerators **24**, 109 (1989).
[8] M. Berz, in *Differential Algebraic Techniques, Entry in 'Handbook of Accelerator Physics and Engineering', M. Tigner and A. Chao (Eds.)* (World Scientific, New York, 1999).
[9] M. Berz, Computer Codes and the Linear Accelerator Community **Los Alamos LA-11857-C**, 137 (1990).
[10] M. Berz, Nuclear Instruments and Methods **A298**, 473 (1990).
[11] K. Makino and M. Berz, Nuclear Instruments and Methods **A427**, 338 (1999).
[12] K. Makino and M. Berz, in *Optical Science, Engineering and Instrumentation '97* (IEEE, SPIE, 1997).
[13] B. Erdelyi, M. Berz, and K. Makino, Technical Report No. MSUCL-1129 (unpublished).

APPENDIX A: STRUCTURE OF B_r AND B_ϕ FOR NON-MAXWELLIAN FIELDS

We start with the Cartesian components

$$B_x(x,y,s) = \sum_{i,j=0}^{n} a_{ij}(s) x^i y^j \qquad B_y(x,y,s) = \sum_{i,j=0}^{n} b_{ij}(s) x^i y^j \tag{A1}$$

as given by the field computation, without imposing any relations among the a_{ij}'s and b_{ij}'s. n is the order of computation. Transformation to cylindrical coordinates gives

$$\begin{aligned} B_r &= B_x \cos\phi + B_y \sin\phi & \qquad B_\phi &= -B_x \sin\phi + B_y \cos\phi \\ x &= r\cos\phi & \qquad y &= r\sin\phi \end{aligned} \tag{A2}$$

Inserting eq. (A1) in eq. (A2) we obtain

$$B_r(r,\phi,s) = \sum_{i,j=0}^{n} r^{i+j} \cos^i\phi \sin^j\phi \,(a_{ij}(s)\cos\phi + b_{ij}(s)\sin\phi) \tag{A3}$$

$$B_\phi(r,\phi,s) = \sum_{i,j=0}^{n} r^{i+j} \cos^i\phi \sin^j\phi \,(-a_{ij}(s)\sin\phi + b_{ij}(s)\cos\phi)$$

The next step is to transform the products of trigonometric functions into a sum of trigonometric functions involving multiple angles

$$\cos^{i+1}\phi\sin^{j}\phi=\sum_{k=0}^{i+j+1}\alpha_k^{(j)}\cos k\phi+\beta_k^{(j)}\sin k\phi \tag{A4}$$
$$\cos^{i}\phi\sin^{j+1}\phi=\sum_{k=0}^{i+j+1}\gamma_k^{(j)}\cos k\phi+\delta_k^{(j)}\sin k\phi$$

where $\alpha_k^{(j)}$, $\beta_k^{(j)}$, $\gamma_k^{(j)}$, $\delta_k^{(j)}$ are real constants depending on j. Hence,

$$B_r=\sum_{i,j=0}^{n}r^{i+j}\left[a_{ij}(s)\sum_{k=0}^{i+j+1}\left(\alpha_k^{(j)}\cos k\phi+\beta_k^{(j)}\sin k\phi\right)+b_{ij}(s)\sum_{k=0}^{i+j+1}\left(\gamma_k^{(j)}\cos k\phi+\delta_k^{(j)}\sin k\phi\right)\right] \tag{A5}$$
$$B_\phi=\sum_{i,j=0}^{n}r^{i+j}\left[-a_{ij}(s)\sum_{k=0}^{i+j+1}\left(\gamma_k^{(j)}\cos k\phi+\delta_k^{(j)}\sin k\phi\right)+b_{ij}(s)\sum_{k=0}^{i+j+1}\left(\alpha_k^{(j)}\cos k\phi+\beta_k^{(j)}\sin k\phi\right)\right]$$

Now we can use the above definition to retain in B_r and B_ϕ just the true multipoles. We need to keep only the terms with $k=i+j+1$, all others giving rise to pseudo-multipoles. We neglect the solenoidal terms, which are always treated best separately from B_s. Then, the components of the field containing just the true multipoles are

$$\tilde{B}_r=\sum_{i,j=0}^{n}r^{i+j}\left[\begin{array}{l}a_{ij}(s)\left(\alpha_{i+j+1}^{(j)}\cos\left(i+j+1\right)\phi+\beta_{i+j+1}^{(j)}\sin\left(i+j+1\right)\phi\right)\\+b_{ij}(s)\left(\gamma_{i+j+1}^{(j)}\cos\left(i+j+1\right)\phi+\delta_{i+j+1}^{(j)}\sin\left(i+j+1\right)\phi\right)\end{array}\right] \tag{A6}$$
$$\tilde{B}_\phi=\sum_{i,j=0}^{n}r^{i+j}\left[\begin{array}{l}-a_{ij}(s)\left(\gamma_{i+j+1}^{(j)}\cos\left(i+j+1\right)\phi+\delta_{i+j+1}^{(j)}\sin\left(i+j+1\right)\phi\right)\\+b_{ij}(s)\left(\alpha_{i+j+1}^{(j)}\cos\left(i+j+1\right)\phi+\beta_{i+j+1}^{(j)}\sin\left(i+j+1\right)\phi\right)\end{array}\right]$$

or by rearranging terms

$$\tilde{B}_r=\sum_{i,j=0}^{n}r^{i+j}\left[\begin{array}{l}\left(a_{ij}(s)\alpha_{i+j+1}^{(j)}+b_{ij}(s)\gamma_{i+j+1}^{(j)}\right)\cos\left(i+j+1\right)\phi\\+\left(a_{ij}(s)\beta_{i+j+1}^{(j)}+b_{ij}(s)\delta_{i+j+1}^{(j)}\right)\sin\left(i+j+1\right)\phi\end{array}\right] \tag{A7}$$
$$\tilde{B}_\phi=\sum_{i,j=0}^{n}r^{i+j}\left[\begin{array}{l}\left(-a_{ij}(s)\gamma_{i+j+1}^{(j)}+b_{ij}(s)\alpha_{i+j+1}^{(j)}\right)\cos\left(i+j+1\right)\phi\\+\left(-a_{ij}(s)\delta_{i+j+1}^{(j)}+b_{ij}(s)\beta_{i+j+1}^{(j)}\right)\sin\left(i+j+1\right)\phi\end{array}\right]$$

By expanding the trigonometric functions in terms of exponentials, it can be seen that: for j even

$$\alpha_{i+j+1}^{(j)}=2^{-(i+j)}\left(-1\right)^{j/2}\qquad\beta_{i+j+1}^{(j)}=0 \tag{A8}$$
$$\gamma_{i+j+1}^{(j)}=0\qquad\delta_{i+j+1}^{(j)}=2^{-(i+j)}\left(-1\right)^{j/2}$$

and for j odd

$$\alpha_{i+j+1}^{(j)}=0\qquad\beta_{i+j+1}^{(j)}=2^{-(i+j)}\left(-1\right)^{(j-1)/2} \tag{A9}$$
$$\gamma_{i+j+1}^{(j)}=-2^{-(i+j)}\left(-1\right)^{(j-1)/2}\qquad\delta_{i+j+1}^{(j)}=0$$

Separation of the double sum into summation over i and j-even, respectively j-odd leads to

$$\tilde{B}_r=\sum_{i=0}^{n}\left\{\begin{array}{l}\sum_{j=0\ j-even}^{n}r^{i+j}\left[a_{ij}(s)\cos\left(i+j+1\right)\phi\right)+b_{ij}(s)\sin(i+j+1)\phi\right]2^{-(i+j)}\left(-1\right)^{j/2}\\+\sum_{j=1\ j-odd}^{n}r^{i+j}\left[-b_{ij}(s)\cos\left(i+j+1\right)\phi\right)+a_{ij}(s)\sin(i+j+1)\phi\right]2^{-(i+j)}\left(-1\right)^{(j-1)/2}\end{array}\right\}$$
$$\tilde{B}_\phi=\sum_{i=0}^{n}\left\{\begin{array}{l}\sum_{j=0\ j-even}^{n}r^{i+j}\left[b_{ij}(s)\cos\left(i+j+1\right)\phi\right)-a_{ij}(s)\sin(i+j+1)\phi\right]2^{-(i+j)}\left(-1\right)^{j/2}\\+\sum_{j=1\ j-odd}^{n}r^{i+j}\left[a_{ij}(s)\cos\left(i+j+1\right)\phi\right)+b_{ij}(s)\sin(i+j+1)\phi\right]2^{-(i+j)}\left(-1\right)^{(j-1)/2}\end{array}\right\} \tag{A10}$$

The symmetry of the above equations should be obvious. $\tilde{B}_r$ and $\tilde{B}_\phi$ have the same number of terms, and if the symmetry holds term by term, then it also holds for their sum. By introducing a new index $l = i + j$ we obtain relations of the form

$$\tilde{B}_r = \sum_{l=0}^{n} \left[A_l(s)\cos(l+1)\phi + B_l(s)\sin(l+1)\phi\right] r^l \tag{A11}$$
$$\tilde{B}_\phi = \sum_{l=0}^{n} \left[B_l(s)\cos(l+1)\phi - A_l(s)\sin(l+1)\phi\right] r^l$$

where $A_l(s)$, $B_l(s)$ are sums over $a_{ij}(s)$, $b_{ij}(s)$ with $i + j = l$. Shifting the origin of summation to make comparison easier with the direct method, and using the convention that the $l = 1$ component corresponds to dipole gives the final form

$$\tilde{B}_r(r,\phi,s) = \sum_{l=1}^{n+1} \left[A_l(s)\cos l\phi + B_l(s)\sin l\phi\right] r^{l-1} \tag{A12}$$
$$\tilde{B}_\phi(r,\phi,s) = \sum_{l=1}^{n+1} \left[B_l(s)\cos l\phi - A_l(s)\sin l\phi\right] r^{l-1}$$

By identification, it is apparent that eq. (A12) is of the same form as the field components derived from a scalar potential, containing only the true multipoles. For example, up to order 5 we can derive the following relations

$$A_1(s) = a_{00}(s) \tag{A13}$$
$$A_2(s) = \frac{1}{2}\left(a_{10}(s) - b_{01}(s)\right) \tag{A14}$$
$$A_3(s) = \frac{1}{4}\left(a_{20}(s) - b_{11}(s) - a_{02}(s)\right) \tag{A15}$$
$$A_4(s) = \frac{1}{8}\left(a_{30}(s) - b_{21}(s) - a_{12}(s) + b_{03}(s)\right) \tag{A16}$$
$$A_5(s) = \frac{1}{16}\left(a_{40}(s) - b_{31}(s) - a_{22}(s) + b_{13}(s) + a_{04}(s)\right) \tag{A17}$$

$$B_1(s) = b_{00}(s) \tag{A18}$$
$$B_2(s) = \frac{1}{2}\left(b_{10}(s) + a_{01}(s)\right) \tag{A19}$$
$$B_3(s) = \frac{1}{4}\left(b_{20}(s) + a_{11}(s) - b_{02}(s)\right) \tag{A20}$$
$$B_4(s) = \frac{1}{8}\left(b_{30}(s) + a_{21}(s) - b_{12}(s) - a_{03}(s)\right) \tag{A21}$$
$$B_5(s) = \frac{1}{16}\left(b_{40}(s) + a_{31}(s) - b_{22}(s) - a_{13}(s) + b_{04}(s)\right) \tag{A22}$$

The differences between the constrained cases (by the Maxwell equations) and arbitrary coefficients now can be analyzed. Obviously, the dipole component will give the same result in every method. The differences start to show up beginning with the quadrupole component. For example the normal quadrupole is given in general by $B_2(s) = \frac{1}{2}\left(b_{10}(s) + a_{01}(s)\right)$.

If we impose $\nabla\cdot\vec{B} = 0$, as it is always the case for magnetic field computations, it gives just $a_{10}(s)+b_{01}(s)+c'_{00}(s) = 0$, that is, it does not impose any constraints between $b_{10}(s)$ and $a_{01}(s)$. On the other hand, if $\nabla\times\vec{B} = 0$, the s component imposes: $b_{10}(s) = a_{01}(s)$. If the curl is not vanishing, i.e. $b_{10}(s) \neq a_{01}(s)$, the method will take as the quadrupole component the average value. The same type of analysis can be performed on higher order multipoles to emphasize the importance of vanishing curl.

As a conclusion, we proved that the method can be used for global Maxwellification, with a unique solution, that alters the original fields by a minimal amount. However, we remind the reader that $\tilde{B}_r$ and $\tilde{B}_\phi$ do not contain all the terms, the whole field expressions for B_r and B_ϕ have contributions from pseudo-multipoles that cannot be written in the form of eq. (22) in case of non-vanishing curl.

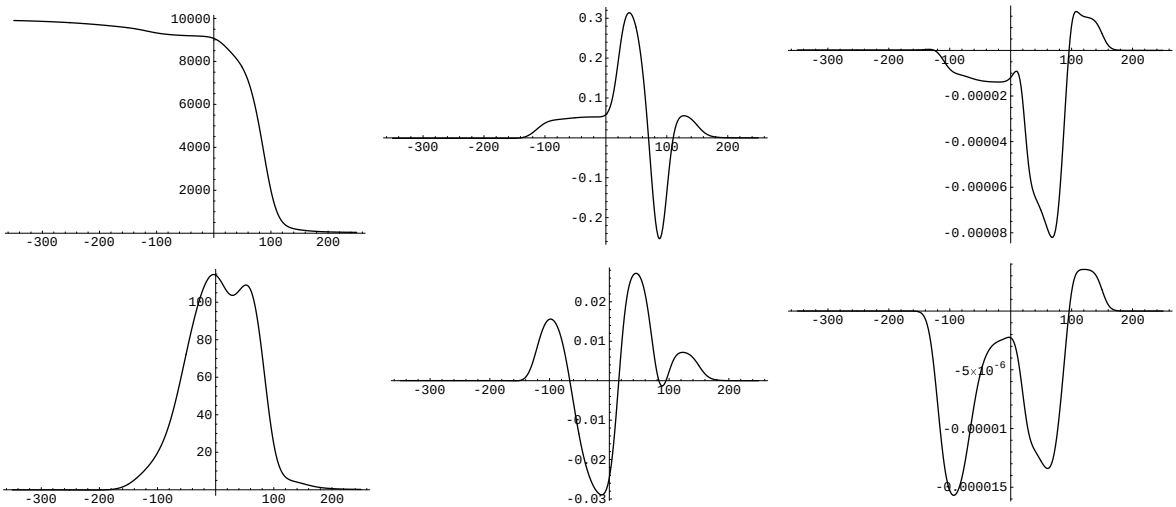

FIG. 1. Multipole strengths of the lead end. Shown are $b_2(s)$, $b_6(s)$, $b_{10}(s)$, $a_2(s)$, $a_6(s)$ and $a_{10}(s)$.

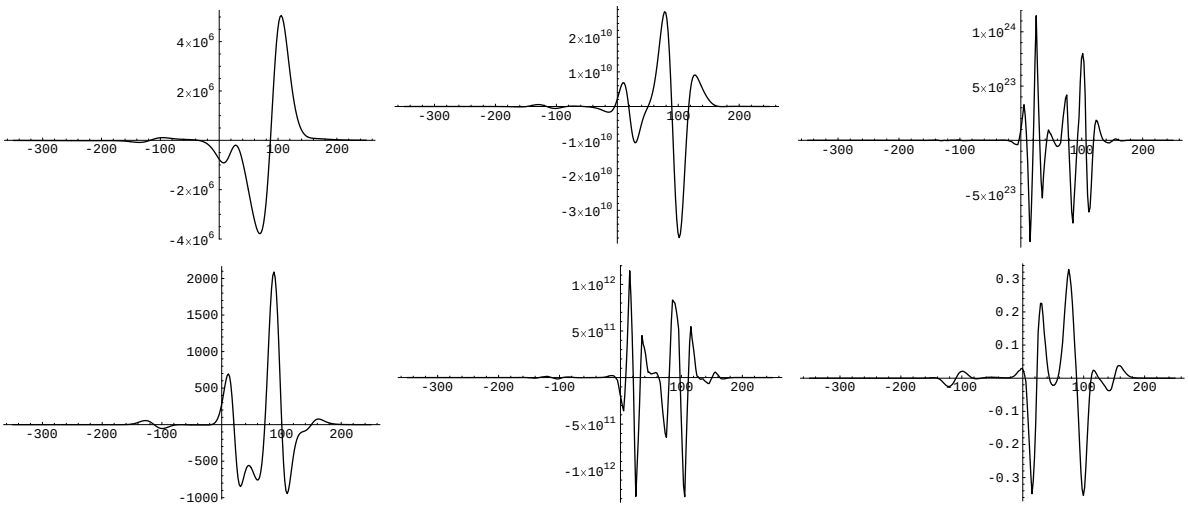

FIG. 2. Normal multipole strengths' s-derivatives of the lead end. Shown are ${b_2}^{(2)}(s)$, ${b_2}^{(4)}(s)$, ${b_2}^{(10)}(s)$, ${b_6}^{(2)}(s)$, ${b_6}^{(6)}(s)$ and ${b_{10}}^{(2)}(s)$.

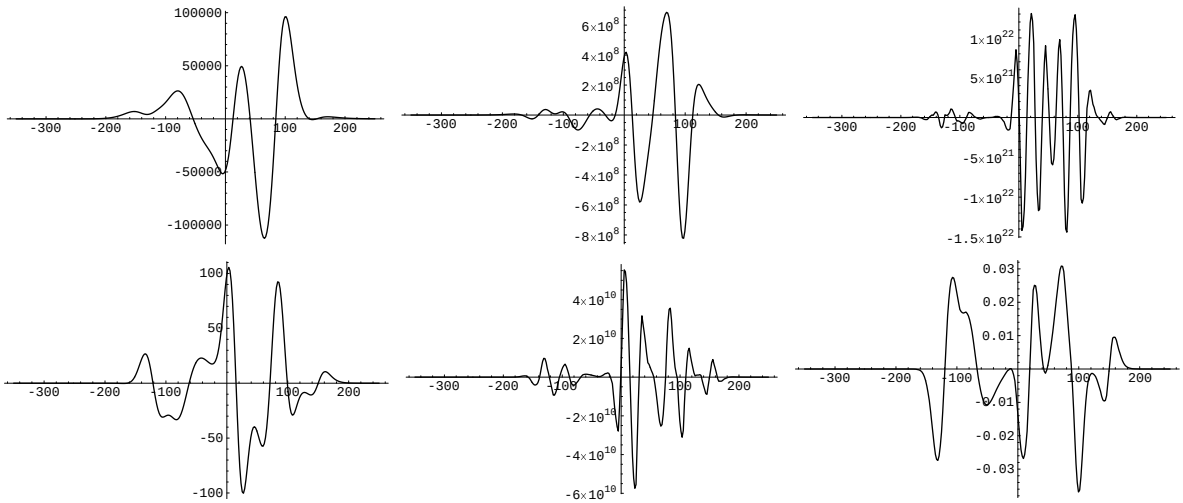

FIG. 3. Skew multipole strengths' s-derivatives of the lead end. Shown are ${a_2}^{(2)}(s)$, ${a_2}^{(4)}(s)$, ${a_2}^{(10)}(s)$, ${a_6}^{(2)}(s)$, ${a_6}^{(6)}(s)$ and ${a_{10}}^{(2)}(s)$.

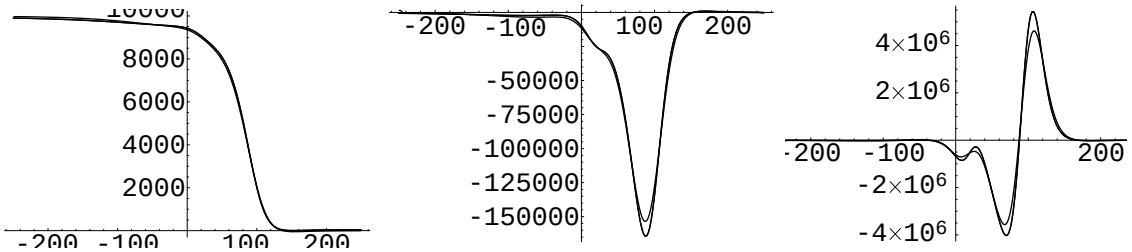

FIG. 4. Normal quadrupole strength, its first and second s-derivatives extracted from Maxwellian and non-Maxwellian fields respectively.

Order	$\frac{\partial^n B_y}{\partial x^n}(0,0,0)$			
n	Computation time [sec]	Max. mem. usage [$bytes$]	Lines of Fortran	Evaluation time [msec]
0	0.02	890672	4	0.3
1	0.09	912192	20	0.8
2	0.33	1025616	69	2.4
3	0.94	1306056	188	7.0
4	2.50	1931872	457	16.0
5	6.26	3213192	1009	36.0
6	12.95	5709304	2078	72.9
7	27.23	10274512	4059	140.9
8	50.16	18590928	7567	267.0
9	96.73	33132056	13603	480.0

TABLE I. Results of transforming the analytic derivatives of the Biot-Savart law calculated with Mathematica to Fortran code.

Order	$\frac{\partial^n B_y}{\partial x^n}(0,0,0)$
n	Evaluation time in μsec up to order n
1	4.8
5	6.8
10	10.7
15	20.5
20	47.8
25	93.7

TABLE II. Computation time of the Taylor expansion of the y-component of the magnetic field in DA at various orders.

$B_x(x,s,y)$			$B_y(x,s,y)$		
Coefficient	Order	Exp. (x,s,y)	Coefficient	Order	Exp. (x,s,y)
0.9384473968456148E-11	0	0 0 0	-.8339510041598585E-11	0	0 0 0
0.1022945817408163E-09	1	1 0 0	17.49010593690617	1	1 0 0
0.1430119891325347E-09	1	0 1 0	-.1304592905872117E-09	1	0 1 0
17.49010593689972	1	0 0 1	0.9584448246993324E-10	1	0 0 1
-.6067419448807509E-09	2	2 0 0	0.5543819518033510E-09	2	2 0 0
0.3602525017014357E-08	2	1 1 0	6 -3.804751735973857	2	1 1 0
0.1205363555495387E-08	2	0 2 0	-.1106863867922359E-08	2	0 2 0
-.2014572349218202E-08	2	1 0 1	0.1941685518966341E-08	2	1 0 1
-3.804751736131598	2	0 1 1	0.3444233784028611E-08	2	0 1 1
-.5986214510200760E-09	2	0 0 2	0.5524820548968856E-09	2	0 0 2
-.2282722315338770E-07	3	3 0 0	-1.666257305421052	3	3 0 0
-.9274588597119049E-09	3	2 1 0	0.1244904457298190E-09	3	2 1 0
0.7183921058029341E-07	3	1 2 0	9.997543895896488	3	1 2 0
0.5557759530372408E-09	3	0 3 0	-.2165498336204053E-10	3	0 3 0
-4.998771979234908	3	2 0 1	-.3052480102017086E-08	3	2 0 1
-.1133153901822226E-06	3	1 1 1	0.1106802772765647E-06	3	1 1 1
9.997543893641829	3	0 2 1	0.6954731157637895E-07	3	0 2 1
-.3357574107631933E-08	3	1 0 2	-4.998771979536424	3	1 0 2
-.7398769930055948E-09	3	0 1 2	-.5953132431457675E-10	3	0 1 2
-1.666257304770050	3	0 0 3	-.2216494703055627E-07	3	0 0 3

TABLE III. Taylor expansion of the magnetic field components B_x and B_y. The columns represent the expansion coefficients, the order in the expansion and the exponents of (x,s,y) respectively.

$\left(\nabla \times \vec{B}\right)_s$ from eq. (10)			$\left(\nabla \times \vec{B}\right)_s$ from eq. (6)		
Coefficient	Order	Exp. (x, s, y)	Coefficient	Order	Exp. (x, s, y)
0.6448175327022909E-11	0	0 0 0	0.6451728040701710E-11	0	0 0 0
0.3123336252824904E-08	1	1 0 0	0.3123335699448115E-08	1	1 0 0
0.1577409314279521E-09	1	0 1 0	0.1577009633990656E-09	1	0 1 0
0.3138928421006493E-08	1	0 0 1	0.3138927988192986E-08	1	0 0 1
0.6297175136893429E-07	2	2 0 0	0.3368312531613524	2	2 0 0
0.1135643710736822E-06	2	1 1 0	0.1135639355887008E-06	2	1 1 0
0.2254658681977162E-08	2	0 2 0	0.2237449336917052E-08	2	0 2 0
0.6101880112296945E-09	2	1 0 1	0.6101442684425235E-09	2	1 0 1
0.1121600312625759E-06	2	0 1 1	0.1121592163033647E-06	2	0 1 1
-.6522627415961324E-07	2	0 0 2	-.3368312554111546	2	0 0 2
-.1035163990081857E-06	3	3 0 0	0.8482986704194671E-06	3	3 0 0
0.3603849257016734E-05	3	2 1 0	-1010523.362231316	3	2 1 0
0.2310457119847342E-05	3	1 2 0	0.4430214737283222E-06	3	1 2 0
0.2364236389995611E-07	3	0 3 0	-.3117654705420136E-04	3	0 3 0
-.1977820552667708E-05	3	2 0 1	-.3840225446083422E-05	3	2 0 1
0.9434835135380232E-08	3	1 1 1	0.9449170335074086E-08	3	1 1 1
0.2256179271853398E-05	3	0 2 1	0.6295506663533956E-05	3	0 2 1
-.1999900781868291E-05	3	1 0 2	-.2090122526610116E-05	3	1 0 2
-.3674740044701252E-05	3	0 1 2	1010523.362276393	3	0 1 2
-.9278849333327333E-07	3	0 0 3	0.5070636007076246E-05	3	0 0 3

TABLE IV. Comparison of the s component of the curl, up to order 3, computed by two different implementation of the Biot-Savart law (eq. (10) and eq. (6) respectively).

$\left(\nabla \times \vec{B}\right)_s$ after Maxwellification		
Coefficient	Order	Exp. (x, s, y)
-.4547473508864641E-12	6	2 0 4
-.1455191522836685E-10	7	2 1 4
0.3051757812500000E-04	8	6 0 2
-.2328306436538696E-09	8	4 2 2
-.3051757812500000E-04	8	2 0 6
0.1862645149230957E-08	9	4 3 2
-.1862645149230957E-08	10	6 2 2
-.1490116119384766E-07	10	4 4 2
-.1490116119384766E-07	10	2 4 4
-.1455191522836685E-10	10	2 0 8
-.2842170943040401E-13	11	5 0 6
0.1490116119384766E-07	11	4 1 6
-.3552713678800501E-14	11	2 0 9
0.5960464477539063E-07	12	2 2 8

TABLE V. The s component of the curl, up to order 12, after Maxwellification of the field in Table III.

Order	Opening aberrations $(x\|a^n)$	
n	Return end	Lead end
2	0	0
3	0.2497609620388847	0.2995410193258450
4	0.6293863605053251E-13	-.3054844395050998E-13
5	0.1903231022089257	0.1962270889999381
6	0.6911276300083234E-12	-.6125473066348172E-12
7	0.1699451387437771	0.9019387229287767E-01
8	-.1364626459777126E-09	0.2013346179046971E-09

TABLE VI. Opening aberrations, $(x|a^n)$, for the return and lead ends' exit focusing maps.